First-Principles Study of a Carbon Nanobud

Xiaojun Wu and Xiao Cheng Zeng*

Department of Chemistry and Nebraska Center for Materials and Nanoscience, University of Nebraska—Lincoln, Lincoln, Nebraska 68588

ABSTRACT Carbon nanobuds (CNBs), a novel carbon nanostructure, have been synthesized recently *via* covalently bonding C_{60} buckyballs to the sidewall of a single-walled carbon nanotube (SWCNT) through cycloaddition reaction [Nasibulin, A. G. *et al.*, *Nat. Nanotechnol.* 2007, *2*, 156]. We perform a first-principles study of structural, electronic, chemical, and field-emission properties of CNBs. It is found that relative stabilities of CNBs depend on the type of carbon—carbon bond dissociated in the cycloaddition reaction. All CNBs are semiconducting regardless of the original SWCNT base being metallic or semiconducting. Chemical attachment of C_{60} to SWCNTs can either open up the band gap (*e.g.*, for armchair SWCNT) or introduce impurity states within the band gap, thereby reducing the band gap (for semiconducting SWCNT). In addition, the band gap of CNBs can be modified by changing the density of C_{60} attached to the sidewall of the SWCNT. The work function of CNBs can be either slightly higher or lower than that of the parent SWCNT, depending on whether the attached SWCNT is armchair or zigzag. Computed reaction pathway for the formation of CNBs shows that the barriers of both forward and backward reactions are quite high, confirming that CNBs are very stable at room temperature.

KEYWORDS: carbon nanobud · C_{60} buckyball · single-walled carbon nanotube · cycloaddition reaction · field emission

The discoveries of low-dimensional carbon nanostructures, such as the "buckyball" C_{60} fullerene in 1985 and the carbon nanotube (CNT) in 1991, have played critical roles in the advancement of modern nanoscience and nanotechnology.[1–6] The C_{60} fullerene is composed of 60 sp^2-hybridized carbon atoms that form a spherical cage, while a single-walled CNT (SWCNT) is essentially a cylindrical graphene sheet composed of sp^2-hybridized carbon atoms. These low-dimensional carbon nanostructures exhibit many unique physical, chemical, and electrical properties, in part due to the quantum-confinement effect. For example, the SWCNT can be either metallic or semiconducting, depending on its helix angle and diameter.[6] Novel properties of C_{60} fullerenes and CNTs endow their promising applications in nanoelectronic devices, sensors, field emission, and composite materials.[1,6,7] Previous experimental studies have shown that the two carbon nanostructures can be actually combined to form hybrid carbon nanostructures. Smith *et al.* have demonstrated that C_{60} fullerenes can be enclosed into CNTs to form the so-called carbon *nanopeapod*, where the interaction between fullerenes and CNTs is of van der Waals type.[8] Both experimental and theoretical studies have shown that electronic properties of nanopeapods are tunable and can be exploited for nanoelectronic applications.[9–20]

More recently, a novel hybrid carbon nanostructure, coined as *carbon nanobud* (CNB), has been successfully synthesized.[21–23] In the CNB, one or more C_{60} fullerene molecules are covalently bonded to the sidewall of a SWCNT. Like many hybrid nanostructures, it is expected that properties of CNBs can be modified by the chemical interaction between C_{60} and the SWCNT or by the density of C_{60} attached to the SWCNT. In fact, an experimental study has shown that CNBs exhibit lower field thresholds and much higher current density than pristine SWCNTs.[21] Furthermore, the attached C_{60} fullerenes yield more space between SWCNTs, thereby weakening the tendency toward adhesion among SWCNTs and preventing formation of tight bundles of SWCNTs. The attached C_{60} may be also used as a molecular support to prevent slipping of SWCNTs in composite materials and to increase the mechanical strength of the materials. Higher chemical reactivity of fullerenes can be exploited for chemically functionalizing CNBs for sensor application. The aim of this article is to investigate various properties of CNBs using a density functional theory method. Particular attention will be placed on the structural, chemical, electronic, and field-

*Address correspondence to xczeng@phase2.unl.edu.

Received for review April 30, 2008 and accepted June 16, 2008.

Published online June 27, 2008.
10.1021/nn800256d CCC: $40.75

© 2008 American Chemical Society

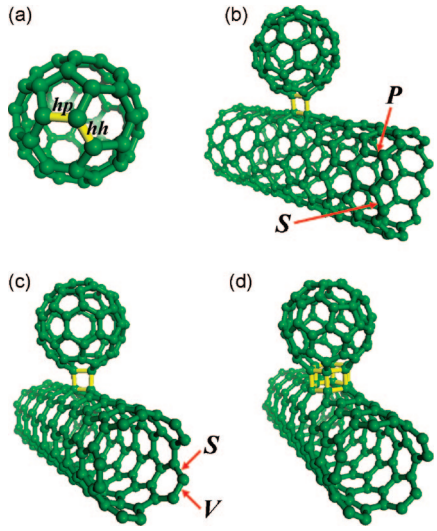

Figure 1. Optimized structures of (a) C_{60} fullerene, and (b–d) CNBs. (b) The *hh* C–C bond in C_{60} and the *P* type C–C bond in the zigzag (10,0) SWCNT form a quadrilateral ring [labeled as "[2 + 2] *hh-P* (zigzag)"]. (c) The *hh* C–C bond in C_{60} and the *S* type C–C bond in the armchair (5,5) SWCNT form a quadrilateral ring [labeled as "[2 + 2] *hh-S* (armchair)"]. (d) A hexagonal face of C_{60} is attached to a hexagonal ring in the armchair (5,5) SWCNT [labeled as "[6 + 6] C_{60}-armchair"].

emission properties. To our knowledge, this is the first comprehensive first-principles study of properties of CNBs.

RESULTS AND DISCUSSION

In the covalent bonding between C_{60} and a SWCNT, our DFT computation shows that a single C–C covalent bond between C_{60} and the SWCNT is unstable and can spontaneously break. At least two C–C covalent bonds are required *via* the cycloaddition reaction to stabilize the CNB (Figure 1b). Two possible ways for the cycloaddition reaction were considered: (1) a pair of parallel C–C bonds form a quadrilateral ring, namely, the [2 + 2] cycloaddition (Figure 1b,c), and (2) a hexagonal face of C_{60} and a hexagonal ring in the SWCNT are connected together to form six C–C covalent bonds, namely, the [6 + 6] cycloaddition (Figure 1d). It is well-known that there exist two types of C–C bonds in C_{60} fullerene, one between two hexagonal faces and another between the hexagonal and pentagonal faces (labeled as the *hh* and *hp* bond in Figure 1a, respectively). Also, two types of C–C bonds can be seen in the SWCNT, characterized by the angle between the C–C bond and the tube axis. Among the C–C bonds, 1/3 are either normal (labeled as *V*) or parallel (labeled as *P*) to the tube axis in the armchair or zigzag SWCNT, while the remaining 2/3 form a sharp angle with the tube axis (labeled *S*), as shown in Figure 1b,c. In total, eight possible C_{60}/SWCNT configurations are available for the [2 + 2] cycloaddition and two C_{60}/SWCNT configurations for the [6 + 6] cycloaddition. We have performed full geometric optimization for all 10 possible C_{60}/SWCNT configurations. The resulting 10 CNB structures are all stable (see Figures S1 and S2 in the Supporting Information). The covalent bonding between C_{60} and SWCNT induces a local distortion of the SWCNT surface where some carbon atoms of the SWCNT are pulled outward from the original wall surface and their bonding is transformed from sp^2- to sp^3-hybridization.

TABLE 1. Binding Energy (E_b), Average Bond Length (l) between C_{60} and SWCNT, and the Charge Transfer per Supercell (q) from C_{60} to SWCNT (The Negative Value of Charge Transfer Means Positive Charges Are Transferred from SWCNT to C_{60})

C_{60}/SWCNT configuration in CNB	E_b (eV)	l (Å)	q (e)
[2 + 2] *hp-V* (armchair)	2.336	1.627	0.013
[2 + 2] *hh-V* (armchair)	1.598	1.619	0.026
[2 + 2] *hh-S* (armchair)	1.461	1.613	−0.028
[2 + 2] *hp-S* (armchair)	2.232	1.617	−0.044
[2 + 2] *hp-P* (zigzag)	2.296	1.606	−0.041
[2 + 2] *hh-P* (zigzag)	1.558	1.605	−0.043
[2 + 2] *hh-S* (zigzag)	1.682	1.625	0.005
[2 + 2] *hp-S* (zigzag)	2.498	1.636	−0.027
[6 + 6] C_{60} armchair	5.950	1.602	0.020
[6 + 6] C_{60} zigzag	6.044	1.596	0.032

The binding energy, average C–C bond length, and the charge transfer per supercell for the 10 C_{60}/SWCNT configurations are summarized in Table 1. The label "[2 + 2] *hh-V* (armchair)" refers to the CNB configuration originating from [2 + 2] cycloaddition reaction between the *hh* C–C bond in C_{60} and the *V* C–C bond in the armchair SWCNT. The binding energy is defined as $E_b = E(\text{CNB}) - E(C_{60}) - E(\text{SWCNT})$, where E is the total energy/supercell. Positive binding energy suggests that the cycloaddition reaction is endothermic. Table 1 shows that CNBs formed *via* the [2 + 2] cycloaddition are more stable than those *via* the [6 + 6] cycloaddition, even though the latter gives rise to six new C–C bonds. For the [2 + 2] cycloaddition, the CNBs associated with the *hh* C–C bond are more stable than those associated with the *hp* C–C bond. The two most stable CNBs are "[2 + 2] *hh-P* (zigzag)" (Figure 1b) and "[2 + 2] *hh-S* (armchair)" (Figure 1c), with C_{60}/SWCNT binding energies of 1.558 and 1.461 eV, respectively.

The relative stabilities among the 10 CNBs can be understood from the π-bonding character of C–C bonds involved in the cycloaddition reaction (also a pericyclic reaction) in which two π bonds are broken while two σ bonds are formed. In C_{60}, the *hh* C–C bond has more π-bonding character than the *hp* C–C bond. In the SWCNT, C–C π bonds are distorted due to the tubular bending, and the degree of distortion is different for the *P*, *V*, and *S* bonds. In the armchair SWCNT, the *V* C–C bonds are more distorted than the *S* C–C bonds, whereas in the zigzag SWCNT, the *P* C–C bonds are less distorted than the *S* C–C bonds. The relative stabilities are also manifested from the average C–C bond length between C_{60} and SWCNT (Table 1). In general, shorter bond length is associated with stronger binding energy.

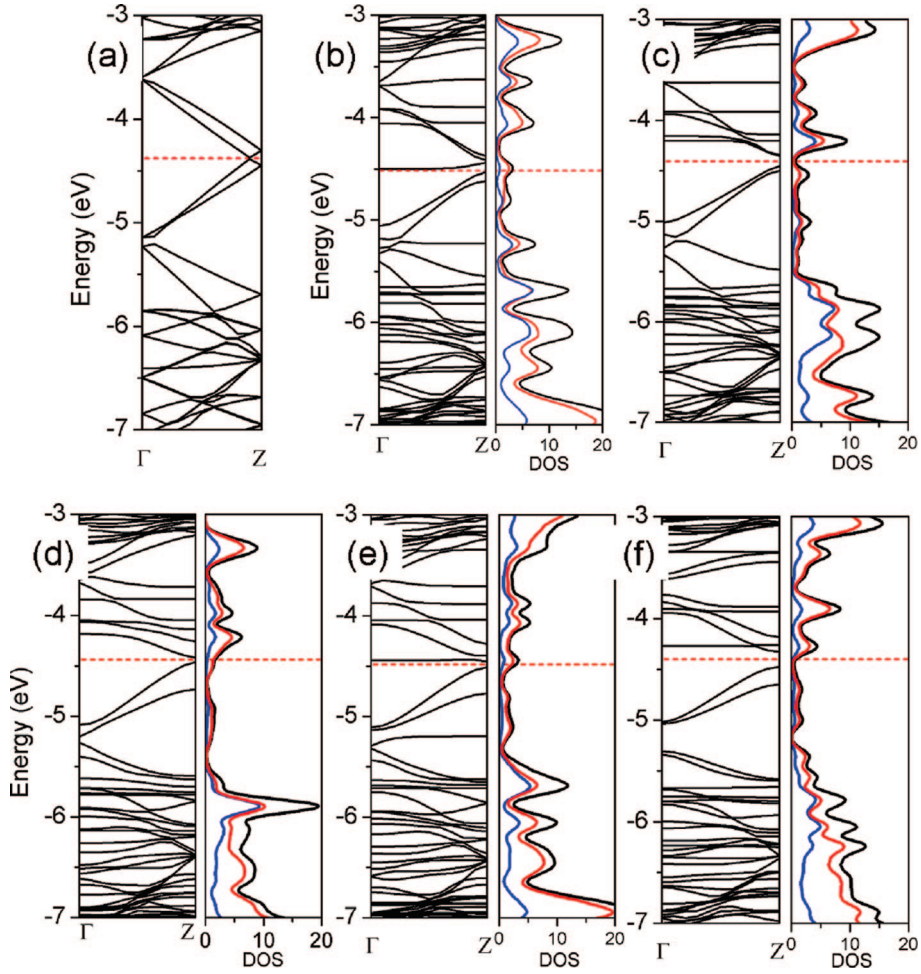

Figure 2. (a) Electronic band structure of pristine armchair (5,5) SWCNT (computed based on eight periodic lengths in the supercell). (b−f) Band structures and DOS of CNBs derived from five different C_{60}/SWCNT configurations: (b) "[2 + 2] *hp-V* (armchair)" configuration; (c) "[2 + 2] *hh-V* (armchair)" configuration; (d) "[2 + 2] *hh-S* (armchair)" configuration; (e) "[2 + 2] *hp-S* (armchair)" configuration; and (f) "[6 + 6] C_{60} armchair" configuration. The Fermi level is plotted with a red dashed line. The projected DOS of C_{60} and SWCNTs are plotted with a blue and red solid line, respectively. The total DOS is plotted with a black solid line.

On the other hand, the CNBs that resulted from the [6 + 6] cycloaddition show shorter bond lengths but much higher binding energies compared to those from the [2 + 2] cycloaddition. A possible reason for this anomaly is that local distortion in the case of [6 + 6] cycloaddition is too large to be compensated by the formation of six new C−C bonds. The charge analysis using the Hirshfeld method indicates that electron transfer between C_{60} and SWCNT can be undertaken in two ways, depending on C_{60}/SWCNT configuration. For the two most stable C_{60}/SWCNT configurations, electrons are transferred from SWCNT to C_{60}. This versatile charge-transfer behavior implies that electronic properties of CNBs may be tunable.

In Figures 2 and 3, electronic band structures and density of states (DOS) of CNBs derived from 10 different C_{60}/SWCNT configurations are presented. Since the CNB has no spin polarization, only the band structures for the majority spin state are displayed. The band structures of perfect armchair (5,5) and zigzag (10,0) SWCNTs are also shown in Figures 2a and 3a. As expected, the band structures show that the armchair (5,5) SWCNT is metallic and the zigzag (10,0) SWCNT is semiconducting with a direct band gap of about 0.8 eV. For C_{60}, the gap between the highest occupied molecular orbital (HOMO) and the lowest unoccupied molecular orbital (LUMO) is 1.67 eV. It is known that the DFT/GGA method generally underestimates the band gap of semiconductors. However, this error does not affect our analysis of electronic properties of CNBs.

The calculated band gaps of CNBs are summarized in Table 2. As shown in Figure 2, upon attachment of C_{60} to the armchair (5,5) SWCNT, a small band gap opens up. The resulting CNBs are semiconducting with the band gap ranging from 0.06 to 0.18 eV. In contrast, previous calculations show that the carbon nanopeapod C_{60}@(10,10) is metallic, with carries distributed either along the (10,10) nanotube or on enclosed C_{60} fullerenes.[10] For CNBs with the zigzag (10,0) SWCNT base, attachment of C_{60} introduces unoccupied impurity states within the band gap. Thus, the resulting CNBs are still semiconducting but with much narrower band

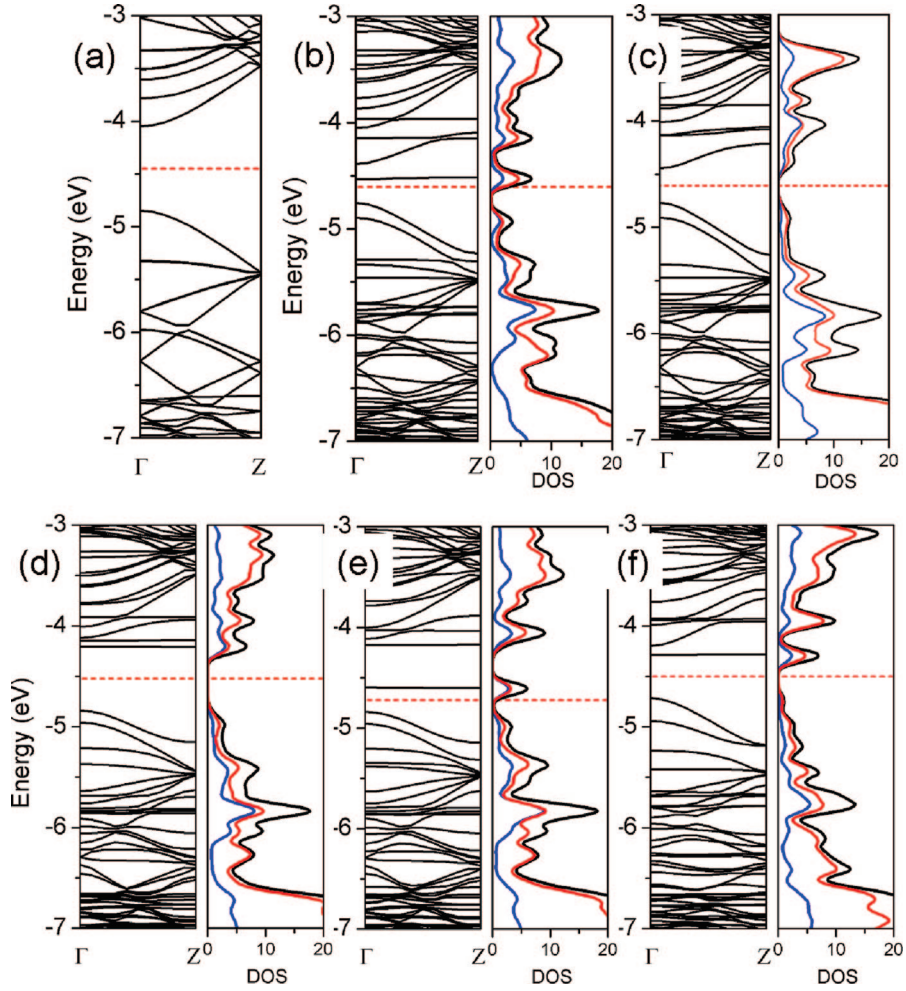

Figure 3. (a) Electronic band structure of pristine zigzag (10,0) SWCNT. (b−f) Band structures and DOS of CNBs derived from five different C_{60}/SWCNT configurations: (b) "[2 + 2] *hp-P* (zigzag)" configuration; (c) "[2 + 2] *hh-P* (zigzag)" configuration; (d) "[2 + 2] *hh-S* (zigzag)" configuration; (e) "[2 + 2] *hp-S* (zigzag)" configuration; and (f) "[6 + 6] C_{60} armchair" configuration. The Fermi level is plotted with a red dashed line. The projected DOS of C_{60} and SWCNTs are plotted with a blue and red solid line, respectively. The total DOS is plotted with a black solid line.

gap (ranging from 0.23 to 0.63 eV) than the pristine (10,0) SWCNT. The CNBs also exhibit some characteristics of an n-type semiconductor. In summary, it appears that all CNBs are semiconducting regardless of original SWCNT base being metallic or semiconducting. In general, the Fermi level of a CNB is slightly lower than that of the parent SWCNT. In addition, by attaching two C_{60} fullerenes to the (5,5) SWCNT within supercell in the "[2 + 2] *hh-S* (armchair)" configuration, the band gap of CNB is further enlarged from 0.1 to 0.22 eV, whereas attaching two C_{60} fullerenes to the (10,0) SWCNT in the "[2 + 2] *hh-P* (zigzag)" configuration results in a smaller band gap of CNB (reduced from 0.35 to 0.17 eV). This result suggests that electronic properties of CNB are highly tunable by changing the C_{60} density on the sidewall of SWCNT.

TABLE 2. Computed Work Function (WF), Band Gap of the CNB and SWCNT, As Well As the Ionization Potential (IP) and HOMO−LUMO Gap ($E_{g(H-L)}$) of C_{60} (The Direct and Indirect Band Gap Are Labeled with $E_{g(D)}$ and $E_{g(I)}$, Respectively)

	WF (eV)	IP (eV)	$E_{g(D)}$ (eV)	$E_{g(I)}$ (eV)	$E_{g(H-L)}$ (eV)
[2 + 2] *hp-V* (armchair)	4.53			0.06	
[2 + 2] *hh-V* (armchair)	4.45		0.17		
[2 + 2] *hh-S* (armchair)	4.46		0.10		
[2 + 2] *hp-S* (armchair)	4.51			0.09	
[6 + 6] C_{60} armchair	4.48		0.18		
[2 + 2] *hp-P* (zigzag)	4.76		0.23		
[2 + 2] *hh-P* (zigzag)	4.77		0.35		
[2 + 2] *hh-S* (zigzag)	4.96			0.63	
[2 + 2] *hp-S* (zigzag)	4.84			0.24	
[6 + 6] C_{60} zigzag	4.72		0.43		
armchair (5,5) SWCNT	4.38		metal		
zigzag (10,0) SWCNT	4.85		0.80		
C_{60}		7.44			1.67

From the projected DOS on C_{60} and the SWCNT (Figures 2 and 3), it can be seen that there is a strong coupling between C_{60} and SWCNT in CNBs, which breaks the symmetry of band structures of the parent SWCNT and induces numerous impurity states near the Fermi level, especially in the region of unoccupied states. For carbon nanopeapods, however, the coupling between

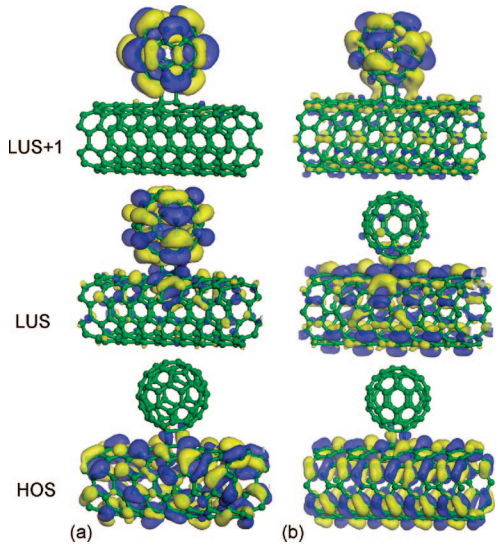

Figure 4. Profiles of the electronic state of HOS, LUS, and LUS+1 at the Γ point for (a) "[2 + 2] *hh-S* (armchair)" and (b) "[2 + 2] *hh-P* (zigzag)" CNBs. The isosurface value is ±0.01 (distinguished by blue/yellow color) in atomic units (au/Bohr^3).

C_{60} and SWCNT is much weaker. Hence, induced impurity states near the Fermi level maintain most of original characteristics of molecular orbitals of C_{60}.[10,20] We have performed a test calculation for C_{60} physisorbed on the outer surface of a SWCNT, where the coupling between C_{60} and the SWCNT is weak. The band structure of this hybrid nanostructure is similar to that of carbon nanopeapods (see Figure S3 in Supporting Information). To learn more about the impurity states, we have plotted electronic profiles of the highest occupied state (HOS), lowest unoccupied state (LUS), and the level above LUS (LUS+1) at the Γ point for all CNBs considered in this study (Figure S4 in Supporting Information). In Figure 4, the electronic profiles of HOS, LUS, and LUS+1 for CNBs in "[2 + 2] *hh-S* (armchair)" and "[2 + 2] *hh-P* (zigzag)" configurations are plotted. The HOS stems mainly from the SWCNT base as well as the two carbon atoms of C_{60} bonded with the SWCNT. For LUS and LUS+1, the carbon atoms of C_{60} make a major contribution. An exception is the LUS of the CNB in the "[2 + 2] *hh-P* (zigzag)" configuration, for which carbon atoms of the SWCNT also make a notable contribution. The induced impurity states due to C_{60} increase possibility of CNBs to be functionalized through chemical reactions with other molecules.

One potential application of CNBs is for cold electron field emission, for which the highly curved C_{60} may act as an emission site when attached to the metallic SWCNT.[21] To evaluate field-emission capability of CNBs, we have estimated the work function (WF) of CNBs. For bulk metals, the WF is given by $\Phi - E_F$, where Φ is the electrostatic potential change across the dipole layer due to the "spilling out of electrons at the metal surface",[24,25] and E_F is the Fermi energy level. For SWCNT, $|\Phi|$ is much smaller than $|E_F|$ due to low density of conduction electrons, and thus WF can be estimated by the value $-E_F$.[26–30] Here, since CNBs are semiconducting with a small band gap, we have used the energy level of conduction band minimum (CBM) to estimate the WF, that is, WF $\approx -E_{CBM}$. In Table 2, the estimated WFs of CBNs and pristine SWCNTs are given. For the purpose of comparison, the ionization potential (IP) of C_{60} fullerene is computed at the same level of theory and is given in Table 2. The WFs of the (5,5) and (10,0) SWCNTs are ~4.38 and 4.85 eV, respectively, slightly less than previous theoretical results obtained from different exchange-correlation functions.[26] Note that the field emission from a SWCNT occurs most likely from its tip. Therefore, to accurately evaluate the WF of a SWCNT, the structure of the tip should be considered. Here, we are mainly concerned with the qualitative difference in WF between CNB and its parent SWCNT. From Table 2, it can be seen that the WF of CNB with the armchair SWCNT base is slightly greater than that of the parent SWCNT, indicating that a higher field threshold is required for the CNB than for its SWCNT base. On the other hand, for the CNB with the zigzag SWCNT base, the change in WF depends on how the C_{60} is attached to the SWCNT. Typically, the WF of the CNB is within a range of [−0.13, +0.11] eV from that of the parent SWCNT. Since C_{60} has little contribution to the HOS, but a large contribution to LUS and LUS+1 (Figure 4), one possible channel for field emission could be that electrons are pumped to the LUS initially and then emit to the vacuum *via* C_{60}.

We note that a previous experimental study has reported that the synthesized CNBs (in water vapor environment) exhibit a low field threshold of ~0.65 V/μm and a much higher current density than pristine SWCNTs synthesized under similar conditions but with no water vapor involved in the synthesis.[21] The apparent discrepancy in the predicted field-emission capability between the experiment and the present theory may be due to the following two reasons: First, the associated water vapor with CNBs in the experiment may effectively reduce the work function of CNBs, a factor not considered in our computation. In fact, Maiti *et al.* have studied the effect of adsorption of water molecules on the field emission of the SWCNT.[28] They found that the adsorption of water molecules can notably reduce the IP of a finite-size SWCNT. Second, the CNTs synthesized in the same experiment may include multiwalled CNTs or may be in bundle form. A number of previous works have shown that multiwalled CNTs or CNT bundles exhibit higher work function than pristine SWCNTs.[26,27,29,30] Future joint experimental and theoretical studies will be needed to examine the dependence of field-emission capability of CNBs on the experimental conditions.

Finally, the reaction pathway for the formation of the CNB from different C_{60}/SWCNT configurations is explored. We have computed the minimum-energy path

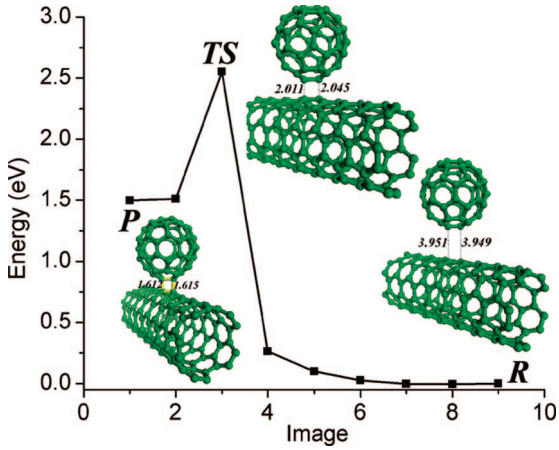

Figure 5. The minimum-energy path for the formation the CNB in the "[2 + 2] *hh-S* (armchair)" configuration. *R*, *TS*, and *P* denote the reactant, transition state, and product, respectively. The energy of the reactant is set to zero. The values of the bond length are in angstroms.

(MEP) for the cycloaddition reaction using the nudged elastic band (NEB) method.[31,32] Briefly, the NEB method can be summarized as the follows: (1) A series of image structures are inserted between the initial and finial state of the reaction. (2) A fictitious spring force is then introduced between all nearest-neighbor image structures. By optimizing these image structures simultaneously, the MEP of the reaction can be obtained, where the real force on the image structures has a zero projection in the direction normal to the MEP. Here, we only present the MEP for the formation of the CNB in the "[2 + 2] *hh-S* (armchair)" configuration in Figure 5. The physisorbed C_{60} on the (5,5) SWCNT is chosen as the reactant (*R*) and the CNB in the "[2 + 2] *hh-S* (armchair)" configuration as the product (*P*). The physisorption energy of C_{60} on the (5,5) SWCNT is −0.038 eV, and the corresponding distance between C_{60} and the (5,5) SWCNT is ~3.95 Å (see bond lengths shown in Figure 5). The MEP indicates that the energy barrier for the formation of the CNB in the "[2 + 2] *hh-S* (armchair)" configuration is about 2.54 eV, while the barrier to dissociation is about 1.04 eV. Thus, the formation process requires a sufficient amount of energy to go over the high-energy barrier. Also, the CNB should be very stable at room temperature due to the relatively high dissociation barrier, as shown also by the experiment.[21] At the transition state (*TS*), the distance between C_{60} and the SWCNT is about 2.01 Å. For comparison, the transition state for the formation of the CNB in the "[2 + 2] *hh-V* (armchair)" and "[2 + 2] *hh-P* (zigzag)" configurations is also searched. Their geometric structures at the transition state are similar to those shown in Figure 5, except C_{60} has a different orientation with respect to the SWCNT base. The computed formation and dissociation barriers are 2.34 and 0.72 eV for "[2 + 2] *hh-V* (armchair)", slightly lower than those for "[2 + 2] *hh-P* (armchair)". For "[2 + 2] *hh-P* (zigzag)", the formation and dissociation barriers are 2.51 and 0.96 eV, respectively, close to those for "[2 + 2] *hh-S* (armchair)".

CONCLUSIONS

We have investigated structural, electronic, chemical, and field-emission properties of CNBs by using the first-principles density functional theory method. It is found that relative stabilities of CNBs depend on the type of carbon−carbon bond dissociated in the cycloaddition reaction. The computed reaction path shows that the formation of the CNBs entails a high-energy barrier in both forward and backward reactions, indicating that CNBs are very stable at room temperature. In general, CNBs are semiconducting regardless of the original SWCNT base being metallic or semiconducting. The band gap of CNB is tunable by changing the density of C_{60} on the sidewall of SWCNT. The induced impurity states in the band gap due to the C_{60} attachment render greater versatility for chemical functionalizing than that of the pristine SWCNTs. The work function of CNBs with the armchair SWCNT base is slightly greater than that of the parent SWCNT, indicating that a higher field threshold is required for field emission with CNBs than that with the SWCNT base. On the other hand, for CNBs with the zigzag SWCNT base, the change in work function depends on relative orientation of C_{60} with respect to SWCNT. Future joint experimental and theoretical studies will be needed to determine the dependence of field-emission capability of CNBs on the synthesis condition and nonvacuum environment. Finally, attachment of C_{60} fullerene molecules to SWCNTs creates more space between SWCNTs, thereby weakening the tendency toward adhesion among SWCNTs. Greater opened space between SWCNTs allows CNBs to be more effective for gas storage.

THEORETICAL METHODS AND MODELS

The first-principles computation was carried out using the linear combination of atomic orbital density functional theory (DFT) method implemented in the DMol3 package.[33−35] The generalized gradient approximation (GGA) in the Perdew−Burke−Ernzerhof (PBE) form and an all-electron double numerical basis set with polarized function (DNP basis set) were chosen for the spin-unrestricted DFT computation.[36] The real-space global cutoff radius was set to be 3.70 Å. For geometric optimization, the forces on all atoms were optimized to be less than 0.05 eV · Å^{-1}. Two SWCNTs were chosen as the base for CNBs, namely, the armchair (5,5) and zigzag (10,0) SWCNT. A tetragonal supercell with a size of 40 × 40 × *c* Å^3 was adopted in the calculation, where *c* is 19.68 Å (eight periodic lengths of the armchair SWCNT) or 21.35 Å (five periodic lengths for the zigzag SWCNT). Each supercell contains one C_{60} fullerene molecule which is covalently bonded to the sidewall of the SWCNT (Figure 1). The nearest distance between two neighboring SWCNTs

is greater than 25 Å, and that between two neighboring C_{60} molecules is greater than 13 Å. Only Γ point was considered in the Brilliouin zone for the geometric optimization. To calculate electronic properties of CNBs, the Brilliouin zone was sampled by $1 \times 1 \times 10$ *k* points using the Monkhorst−Pack scheme.[37]

Acknowledgment. This work is supported by grants from the DOE (DE-FG02-04ER46164), NSF (CHE-0427746, CHE-0701540, and CMMI-0709333), the Nebraska Research Initiative, NSFC (#20628304), and by the Research Computing Facility at the University of Nebraska−Lincoln, and Holland Computing Center at the University of Nebraska−Omaha.

Supporting Information Available: Optimized structures of CNBs with the armchair (5,5) SWCNT base, optimized structures of CNBs with the zigzag (10,0) SWCNT base, band structure of C_{60} physisorbed on the armchair (5,5) SWCNT, and profiles of HOS, LUS, and LUS+1 of CNBs at Γ point. This material is available free of charge *via* the Internet at http://pubs.acs.org.

REFERENCES AND NOTES

1. Dresselhaus, M. S.; Dresselhaus, G.; Eklund, P. C. *Science of Fullerences and Carbon Nanotubes*; Academic Press: New York, 1996.
2. Kroto, H. W.; Heath, J. R.; O'Brien, S. C.; Curl, R. F.; Smalley, R. E. C_{60}: Buckminsterfullerene. *Nature* **1985**, *318*, 162–163.
3. Iijima, S. Helical Microtubules of Graphitic Carbon. *Nature* **1991**, *354*, 56–58.
4. Beghune, D. S.; Kiang, C. H.; de Vries, M. S.; Gorman, G.; Savoy, R.; Vazquez, J.; Beyers, R. Cobalt-Catalysed Growth of Carbon Nanotubes with Single-Atomic-Layer Walls. *Nature* **1993**, *363*, 605–607.
5. Louie, S. G. Electronic Properties, Junctions, and Defects of Carbon Nanotubes. *Top. Appl. Phys.* **2001**, *80*, 113–145.
6. Baughman, R. H.; Zakhidov, A. A.; de Heer, W. A. Carbon Nanotubes—The Route Toward Applications. *Science* **2002**, *297*, 787–792.
7. Hou, T.-H.; Raza, H.; Afshari, K.; Ruebusch, D. J.; Kan, E. C. Nonvolatile Memory with Molecular-Engineered Tunneling Barriers. *Appl. Phys. Lett.* **2008**, *92*, 153109.
8. Smith, B. W.; Monthioux, M.; Luzzi, D. E. Encapsulated C_{60} in Carbon Nanotubes. *Nature* **1998**, 323–324.
9. Lee, J.; Kim, H.; Kahng, S.-J.; Kim., G.; Son, Y.-W.; Ihm, J.; Kato, H.; Wang, Z. W.; Okazaki, T.; Shinohara, H.; Kuk, Y. Bandgap Modulation of Carbon Nanotubes by Encapsulated Metallofullerenes. *Nature* **2002**, *415*, 1005–1008.
10. Hornbaker, D. J.; Kahng, S.-J.; Misra, S.; Smith, B. W.; Johnson, A. T.; Mele, E. J.; Luzzi, D. E.; Yazdani, A. Mapping the One-Dimensional Electronic States of Nanotube Peapod Structures. *Science* **2002**, *295*, 828–831.
11. Okada, S.; Saito, S.; Oshiyama, A. Energetics and Electronic Structures of Encapsulated C_{60} in a Carbon Nanotube. *Phys. Rev. Lett.* **2001**, *86*, 3835–3838.
12. Okada, S.; Otani, M.; Oshiyama, A. Electron-State Control of Carbon Nanotubes by Space and Encapsulated Fullerenes. *Phys. Rev. B* **2003**, *67*, 205411.
13. Liu, X.; Pichler, T.; Knupfer, M.; Golden, M. S.; Fink, J.; Kataura, H.; Achiba, Y.; Hirahara, K.; Iijima, S. Filling Factors, Structural, and Electronics of C_{60} Molecules in Single-Wall Carbon Nanotubes. *Phys. Rev. B* **2002**, *65*, 045419.
14. Du, M. H.; Cheng, H. P. Manipulation of Fullerene-Induced Impurity States in Carbon Peapods. *Phys. Rev. B* **2003**, *68*, 113402.
15. Pichler, T.; Kuzmany, H.; Kataura, H.; Achiba, Y. Metallic Polymers of C_{60} Inside Single-Walled Carbon Nanotubes. *Phys. Rev. Lett.* **2001**, *87*, 267401.
16. Simon, F.; Kuzmany, H.; Náfrádi, B.; Fehér, T.; Forró, L.; Fülöp, F.; Jánossy, A.; Korecz, L.; Rockenbauer, A.; Hauke, F.; et al. Magnetic Fullerenes Inside Single-Wall Carbon Nanotubes. *Phys. Rev. Lett.* **2006**, *97*, 136801.
17. Liu, Z.; Koshino, M.; Suenaga, K.; Mrzel, A.; Kataura, H.; Iijima, S. Transmission Electron Microscopy Imagination of Individual Functional Groups of Fullerene Derivatives. *Phys. Rev. Lett.* **2006**, *96*, 088304.
18. Hirahara, K.; Suenaga, K.; Bandow, S.; Kato, H.; Okazaki, T.; Shinohara, H.; Iijima, S. One-Dimensional Metallofullerene Crystal Generated Inside Single-Walled Carbon Nanotubes. *Phys. Rev. Lett.* **2000**, *85*, 5384–5387.
19. Guan, L. H.; Suenaga, K.; Shi, Z. S.; Gu, Z. N.; Iijima, S. Directed Imagining of the Alkali Metal Site in K-Doped Fullerene Peapods. *Phys. Rev. Lett.* **2005**, *94*, 045502.
20. Dubay, O.; Kresse, G. Density Functional Calculations for C_{60} Peapods. *Phys. Rev. B* **2004**, *70*, 165424.
21. Nasibulin, A. G.; Pikhitsa, P. V.; Jiang, H.; Brown, D. P.; Krasheninnikov, A. V.; Anisimov, A. S.; Queipo, P.; Moisala, A.; Gonzalez, D.; Lientschnig, G.; et al. A Novel Hybrid Carbon Material. *Nat. Nanotechnol.* **2007**, *2*, 156–161.
22. Li, X. L.; Liu, L. Q.; Qin, Y. J.; Wu, W.; Guo, Z. X.; Dai, L. M.; Zhu, D. B. C_{60} Modified Single-Walled Carbon Nanotubes. *Chem. Phys. Lett.* **2003**, *377*, 32–36.
23. Nasibulin, A. G.; Anisimov, A. S.; Pikhitsa, P. V.; Jiang, H.; Brown, D. P.; Choi, M.; Kauppinen, E. I. Investigations of NanoBud Formation. *Chem. Phys. Lett.* **2007**, *446*, 109–114.
24. Lang, N. D.; Kohn, W. Theory of Metal Surfaces: Work Function. *Phys. Rev. B* **1971**, *3*, 1215–1223.
25. Skriver, H. L.; Rosengaard, N. M. Surface-Energy agnd Work Function of Elemental Metals. *Phys. Rev. B* **1992**, *46*, 7157–7168.
26. Zhou, G.; Duan, W. H.; Gu, B. L. Electronic Structure and Field-Emission Characteristics of Open-Ended Single-Walled Carbon Nanotubes. *Phys. Rev. Lett.* **2001**, *87*, 095504.
27. Zhao, J. J.; Han, J.; Lu, J. P. Work Functions of Pristine and Alkali-Metal Intercalated Carbon Nanotubes and Bundles. *Phys. Rev. B* **2002**, *65*, 193401.
28. Maiti, A.; Andzelm, J.; Tanpipat, N.; Allmen, P. v. Effect of Adsorbates on Field Emission from Carbon Nanotubes. *Phys. Rev. Lett.* **2001**, *87*, 155502.
29. Groning, O.; Kuttel, O. M.; Emmenegger, C.; Groning, P.; Schlapbach, L. Field Emission Properties of Carbon Nanotubes. *J. Vac. Sci. Technol.* **2000**, *18*, 665–670.
30. Suzuki, S.; Bower, C.; Watanabe, Y.; Zhou, O. Work Functions and Valence Band State of Pristine and Cs-Intercalated Single-Walled Carbon Nanotube Bundles. *Appl. Phys. Lett.* **2000**, *76*, 4007–4009.
31. Henkelman, G.; Jósson, H. Improved Tangent Estimate in the Nudged Elastic Band Method for Finding Minimum Energy Paths and Saddle Points. *J. Chem. Phys.* **2000**, *113*, 9978–9985.
32. Olsen, R. A.; Kroes, G. J.; Henkelman, G.; Arnaldsson, A.; Jósson, H. Comparison of Methods for Finding Saddle Points without Knowledge of the Final States. *J. Chem. Phys.* **2004**, *121*, 9776–9792.
33. Delley, B. An All-Electron Numerical Method for Solving the Local Density Functional for Polyatomic Molecules. *J. Chem. Phys.* **1990**, *92*, 508–517.
34. Delley, B. From Moelcules to Solids with the DMol3 Approach. *J. Chem. Phys.* **2003**, *113*, 7756–7764.
35. DMol3 is a density functional theory quantum mechanical package available from Accelrys Software Inc.
36. Perdew, J. P.; Burke, K.; Ernzerhof, M. Generalized Gradient Approximation Made Simple. *Phys. Rev. Lett.* **1996**, *77*, 3865–3868.
37. Monkhorst, H. J.; Pack, J. D. Special Points for Brillouin-Zone Integrations. *Phys. Rev. B* **1976**, *13*, 5188–5192.